Polar amplification in idealized climates: the role of ice, moisture, and seasons

Nicole Feldl[1], Timothy M. Merlis[2]

[1]Department of Earth and Planetary Sciences, University of California, Santa Cruz, California, USA
[2]Department of Atmospheric and Oceanic Sciences, McGill University, Montreal, Quebec, Canada

Key Points:

- Annual-mean polar amplification is insensitive to the inclusion of a seasonal cycle of insolation with a simple ice-albedo feedback.
- Fidelity of the seasonality of polar warming occurs under the combined influence of seasons and thermodynamic-ice processes.
- The ice-albedo feedback and moist energy transport make comparable and nearly additive contributions to polar-amplified warming.

Corresponding author: Nicole Feldl, `nfeldl@ucsc.edu`

Abstract

Polar amplification is simulated across models of various complexities, yet uncertainty in attribution remains due to interactions among local feedbacks and poleward energy transports. Here, the role of sea-ice processes, moist energy transport, and the seasonal cycle of insolation are systematically investigated in two models, an energy balance model and an idealized general circulation model. Compared to a simple ice-albedo feedback, seasonal polar warming and transport changes are profoundly affected by the combined influence of seasons and thermodynamic-ice processes. A summer warming minimum occurs where temperatures are in their melting regime, and a maximum occurs where thick, cold ice preconditions a large radiatively forced response. Despite this enhanced winter warming, the annual-mean polar amplification is modestly reduced. When latent heat transport is disabled, polar amplification is further reduced by a factor of 1.7 across the range of ice representations, suggestive of a superposition of warming by ice and moist processes.

Plain Language Summary

Since the 1970s, simulations of climate change have predicted warming that is greatest in polar regions. This polar-amplified warming is ubiquitous, though uncertain in magnitude, in climate models subjected to increases in greenhouse gases and has been variously attributed to the ice-albedo feedback, associated with the retreat of reflective sea ice; the lapse rate feedback, associated with the uneven warming of the Arctic atmosphere; and changes in heat transport by atmospheric circulations. In this study, we turn to highly simplified climate models to isolate the role of sea ice, moisture, and seasons on polar amplification and to explore their interactions. We find that, in order to reproduce the seasonality of polar warming in a manner consistent with both observations and state-of-the-art climate models, it is necessary to model the changing thickness of sea ice and not just its retreat. This effect works in concert with moisture transport by the atmosphere to further enhance polar amplification. Together, the findings imply that sea-ice loss leads to winter warming that would promote a lapse rate feedback and that the increase in moist energy transport would also lead, in more complex models, to additional warming by increasing the water-vapor greenhouse effect.

1 Introduction

Polar amplification has been a robust projection since the earliest climate simulations; nevertheless, the magnitude and timing of the surface warming at high latitudes remains poorly constrained. The phenomenon has been variously attributed to the ice-albedo feedback (e.g., Manabe & Wetherald, 1975), to an increase in poleward atmosphere-ocean energy transport (e.g., Holland & Bitz, 2003; Hwang et al., 2011), and to temperature feedbacks (e.g., Winton, 2006; Pithan & Mauritsen, 2014); recent work has highlighted the interconnected nature of the summertime and wintertime feedbacks over sea-ice regions (Boeke & Taylor, 2018; Dai et al., 2019; Feldl et al., 2020). Hence the uncertainty in projections of climate change, commonly expressed as intermodel spread, arises in part from incomplete understanding of the interaction among these processes. While simple models tend to emphasize that poleward energy transport *can* produce polar-amplified warming purely through moist atmospheric processes (e.g., Roe et al., 2015; Merlis & Henry, 2018), they often neglect critical real-world physics such as ice thermodynamics and seasonal variations in insolation. Investigation of a current gap in the modeling hierarchy—that of the idealized moist, icy, and seasonal climate model—reveals how energy transport and sea-ice processes work in concert to produce latitudinally and seasonally varying warming.

For our idealized climate models, we consider both energy balance models (EBMs) and general circulation models (GCMs). Traditional EBMs represent atmospheric energy transport as a diffusive process proportional to the meridional gradient of temperature and include the ice-albedo feedback via a temperature-dependent surface albedo (Budyko, 1969; Sellers, 1969; North, 1975; North et al., 1981). As a consequence of these parametrizations, when subject to a uniform radiative forcing, the simulated warming is greatest at polar latitudes. When the ice albedo is locked (Merlis, 2014) or the surface-albedo feedback disabled (Armour et al., 2019), warming is uniform, and every latitude warms by the reference climate sensitivity. Thus polar amplification in the dry EBM requires spatial heterogeneity in radiative feedbacks or radiative forcing in order to drive changes in atmospheric energy transport. The results of the early modeling studies in particular have contributed to the prevailing view that polar amplification requires the presence of sea-ice processes.

The rise of the moist EBM in recent years has challenged the necessity of polar feedbacks in producing polar-amplified warming. In the moist EBM, moist static energy replaces temperature in the calculation of diffusive energy transport, which allows for an increase in the latent component of energy transport with warming (Flannery, 1984). Accounting for the effects of latent heat on energy transport improves the ability of EBMs to mimic the zonal-mean behavior of GCMs. Further, in contrast to their dry counterparts, moist EBMs produce polar amplification even in the absence of spatially varying radiative forcing or feedbacks (Roe et al., 2015). This behavior can be understood as a result of the preferential increase in tropical water vapor with warming that, combined with down-gradient moist static energy diffusion, produces an increase in atmospheric energy transport. Moist EBMs can be coupled to a sea-ice parametrization (e.g., Lutsko et al., 2020), prescribed with surface albedo changes (e.g., Hwang & Frierson, 2010), or neither (e.g., Merlis & Henry, 2018). Not surprisingly, when the ice-albedo feedback is enabled in one form or another, polar amplification is enhanced. We also note that two varieties of the moist EBM implementation are in common usage: a climatological version that integrates the governing equation numerically and does not prescribe patterns of feedbacks (Frierson et al., 2007; Merlis & Henry, 2018) and a perturbation version cast in terms of meridional patterns of radiative forcing, radiative feedbacks, ocean heat uptake, and anomalous moist static energy (Rose et al., 2014; Roe et al., 2015; Bonan et al., 2018; Armour et al., 2019). In this study we build upon the former so that sea ice is an interactive component of the climate system, allowing it to shape the control climate and the response to warming.

Like moist EBMs, idealized GCMs are capable of producing polar amplification in the absence of sea-ice processes (Alexeev et al., 2005; Langen et al., 2012; Russotto & Biasutti, 2020), though the result is not ubiquitous and is likely model dependent (Feldl et al., 2017). For instance, Kim et al. (2018) showed that an aquaplanet simulation with clouds, seasonally varying insolation, and no ice-albedo feedback results in a notable lack of polar amplification, due to cancellation by polar cloud feedbacks, whereas under perpetual equinox conditions the otherwise identical model exhibits a strongly polar-amplified response due to increased atmospheric stability in polar regions. A number of questions arise regarding the fundamental role of seasonality in polar amplification that, given the disparity of previous results, warrant systematic investigation: Does the seasonal cycle of insolation affect annual-mean polar amplification in highly idealized models? What accounts for the seasonality of polar amplification itself? Further, given that sea-ice thermodynamic processes are known to stabilize the climate (e.g., Bitz & Roe, 2004; Eisenman & Wettlaufer, 2009), how important are thermodynamic processes associated with the seasonal cycle of sea-ice thickness in simulating polar amplification?

Evidence from models of various complexities suggest that local climate feedbacks work in concert with moist atmospheric processes to consistently produce polar-amplified warming. In what follows, we investigate the sensitivity of the warming pattern to the seasonal cycle and to sea-ice physics. We advance prior studies of annual-mean polar amplification by incorporating the seasonal dynamics of sea ice in our EBM and idealized

GCM, following the work of Wagner and Eisenman (2015) on sea-ice instability, such that we may consider both ice-thickness and ice-albedo effects. Of particular interest is the potential for additivity of the different mechanisms contributing to polar amplification. In other words, we seek to determine how the magnitude of polar amplification is controlled by ice and moist-transport processes both combined and in isolation.

2 Methods

2.1 Moist EBM

The EBM used in this study, at its most comprehensive level, includes seasonal variations in climate, an idealized representation of sea-ice thickness and albedo, and an idealized representation of atmospheric energy transport as a moist diffusive process. The model evolves surface enthalphy, $E(x,t)$ where x is sine of latitude, which represents the energy stored in the ocean mixed layer as sensible heat when the ocean is ice free or in sea ice as latent heat when the ocean is ice covered. For ice-free conditions, the governing equation is

$$c_w \frac{\partial T}{\partial t} = aS - (A + BT) - \nabla \cdot F_a + \mathcal{F} \tag{1}$$

with mixed-layer heat capacity c_w, surface temperature T, net solar radiation aS, outgoing longwave radiation (OLR) $A+BT$, divergence of atmospheric energy transport $\nabla \cdot F_a$, and uniform radiative forcing $\mathcal{F}$. Net solar radiation follows Wagner and Eisenman (2015), where insolation $S(x,t) = S_0 - S_1 x \cos \omega t - S_2 x^2$. The fraction of insolation that is absorbed, a, depends on solar zenith angle, cloudiness, and surface albedo, which we approximate as $a_0 - a_2 x^2$ where $E \geq 0$ (open-water conditions) and a_i where $E < 0$ (ice). We use the following parameter values: $c_w = 7.8$ W yr m^{-2} K^{-1} (i.e., equivalent to a mixed-layer depth of 60 m), $A = 195$ W m^{-2}, $B = 1.8$ W m^{-2}, $S_0 = 420$ W m^{-2}, $S_1 = 290$ W m^{-2}, and $S_2 = 240$ W m^{-2}, $a_0 = 0.7$, $a_2 = 0.1$, and $a_i = 0.4$. In the control simulation, $\mathcal{F} = 0$ W m^{-2}, and it is increased to $\mathcal{F} = 8$ W m^{-2} in the perturbation simulation. The magnitude of the forcing, roughly comparable to a 4$\times$ CO_2 scenario, is sufficient to for the climate to become ice-free, though the results are qualitatively similar for a smaller amplitude forcing that retains winter ice.

Divergence of atmospheric energy transport is assumed to be proportional to the meridional gradient of near-surface moist static energy (MSE) h:

$$\nabla \cdot F_a(x) = -\frac{\partial}{\partial x} D(1 - x^2) \frac{\partial h}{\partial x}, \tag{2}$$

with constant diffusivity $D = 0.3$ W m^{-2} K^{-1}. Building on the work of Wagner and Eisenman (2015), diffusion occurs in a ghost layer with heat capacity $c_g = 0.098$ W yr m^{-2} K^{-1}; the ghost-layer temperature T_g is relaxed to the surface temperature with time scale $\tau_g = 1 \times 10^{-5}$ yr and evolves according to

$$c_g \frac{\partial T_g}{\partial t} = \frac{c_g}{\tau_g}(T - T_g) + D\nabla^2 h. \tag{3}$$

MSE is defined in units of temperature as $h = T_g + c_p^{-1} L_v \mathcal{H} q_s(T_g)$ for latent heat of vaporization $L_v = 2.5 \times 10^6$ J kg^{-1}, relative humidity $\mathcal{H} = 0.8$, heat capacity of air at constant pressure $c_p = 1004.6$ J kg^{-1} K^{-1}, and saturation vapor pressure q_s. Numerically, this approach enables us to perform a semi-implicit time-stepping method on T_g, in contrast to the forward Euler method performed on T, though we note saturation specific humidity is calculated on the previous time step for convenience. Alternatively, MSE can be linearized about a spatially varying climatological temperature (e.g., Merlis & Henry, 2018) to have a more thoroughly semi-implicit time discretization, which produces indistinguishable results.

Sea-ice thickness, h_i is governed by the balance between the vertical heat flux upward through the ice and the surface energy flux

$$\frac{k(T_m - T_0)}{h_i} = -aS + A + B(T_0 - T_m) + \nabla \cdot F_a - \mathcal{F}, \tag{4}$$

with ice thermal conductivity $k = 2$ W m^{-1} K^{-1} and melting point $T_m = 0°$C (Wagner & Eisenman, 2015). From Equation 4, we obtain the freezing temperature of ice, T_0, used to determine the ice regime. In the freezing regime, $T_0 < T_m$ and $E < 0$; the energy flux is balanced by subfreezing surface temperature, and $T = T_0$. In the melting regime, $T_0 \geq T_m$ and $E < 0$, and surface temperature remains at the melting point, $T = T_m$. Open-water conditions are included by adding a third surface temperature regime: if $E \geq 0$, $T = E/c_w$, and (1) governs the surface's evolution.

The model is integrated numerically over the domain $-1 < x < 1$ with 120 grid points spaced uniformly in x and 1000 time steps per year.

2.2 GCM

The idealized moist GCM builds on the work of Frierson et al. (2006) and includes a gray-radiation atmosphere and an idealized hydrological cycle. Water vapor is advected by the resolved-scale flow, undergoing condensation when supersaturated, and is subject to a simple moist convection parameterization for unresolved convection (Frierson et al., 2007). Insolation varies seasonally according to a circular orbit with Earth's obliquity (23.45°) and a 360-day year. A top-of-atmosphere coalbedo that is a time-independent function of latitude ϕ is given by $a^{TOA} = a_0^{TOA} + \Delta a^{TOA}(3\sin^2\phi - 1)/2$, which represents the atmosphere's contribution, primarily clouds, to the planetary albedo. We use $a_0^{TOA} = 0.68$ and $\Delta a^{TOA} = -0.2$, following North et al. (1981). An additional, temperature-dependent surface albedo is applied with a value of 0.4 for sub-freezing temperatures and 0.1 otherwise. The surface boundary condition follows the formulation described above for the EBM, as implemented by Zhang et al. (submitted). Climate changes are forced by varying the longwave optical depth in the gray radiation scheme (O'Gorman & Schneider, 2008). The control simulation optical depth at the surface varies meridionally, according to $\tau_e + (\tau_p - \tau_e)\sin^2\phi$, with $\tau_e = 7.2$ and $\tau_p = 3.6$. The vertical structure of the optical depth is the same as in O'Gorman and Schneider (2008), and the perturbation simulations have a 50% larger optical depth. As in the perturbed EBM climates, this is a sufficient amplitude forcing for the GCM climate to enter a perennial ice-free state.

The GCM simulations use T42 spectral resolution ($\approx 2.8°$ horizontal resolution) with 30 vertical levels. They are integrated for 30 years with a 600 s timestep, and we present averages over the last 20 years.

The GCM closely follows the EBM formulation with the following differences. The insolation and prescribed planetary albedo differ somewhat, though control values of absorbed solar radiation at the top-of-atmosphere are in good agreement (Fig. S1). The GCM atmosphere explicitly simulates atmosphere's large-scale turbulence, in ways that potentially depart from the constant diffusivity formulation of the EBM. The GCM atmosphere additionally has full vertical structure, including a representation of moist convection. This allows for spatially varying lapse rate feedback. As a result of these differences, the GCM has a more stable temperature feedback and a weaker destabilizing ice albedo feedback than the corresponding EBM, and hence the magnitude of the global-mean radiative forcing is roughly three times that of the EBM to produce a comparable climate response.

2.3 Experiment Hierarchy

The models described above are the most comprehensive versions of the "Moist EBM" and GCM presented in this study. Further, we incrementally disable ice thermodynamics, the seasonal cycle of insolation, ice albedo, and the effect of latent energy on the EBM's diffusive representation of atmospheric energy transport in order to assess their relative contributions to polar amplification in our idealized framework:

- *Ice thermodynamics* - Our most comprehensive simulations. In addition to an ice-thickness-dependent surface temperature, they also include a temperature-dependent albedo and hence an ice-albedo feedback.
- *Simple ice-albedo feedback* - Sea-ice thermodynamics are eliminated while retaining the surface-albedo temperature dependence $\alpha(T)$ by evolving the surface enthalpy assuming a surface of 60 m of water and permitting sub-freezing temperatures. Hence, surface temperature is given everywhere by the open-water condition (E/c_w).
- The seasonal cycle is eliminated from the EBM by setting $S_1 = 0$ W m^{-2} and by using the annual-mean of the seasonal insolation for all times in the GCM.
- *Ice-free* - Ice albedo and ice thermodynamics are both eliminated by setting the albedo equal to its spatially varying open-water value.
- *"Dry EBM"* - In the case of the EBM, the effect of latent energy is eliminated by setting $\mathcal{H} = 0$. As is typical, the diffusivity D is doubled to 0.6 W m^{-2} K^{-1} to maintain an Earth-like atmospheric energy transport (Flannery, 1984). The Dry EBM is identical to that of Wagner and Eisenman (2015), aside from certain parameter values and a global, rather than single-hemisphere, domain.

For the Dry EBM, we use a control radiative forcing of $\mathcal{F} = 2$ W m^{-2} to represent a comparable mean-state to the Moist EBM, and it is increased to $\mathcal{F} = 10$ W m^{-2} in the perturbation simulation. Ice thermodynamics, the seasonal cycle of insolation, and ice albedo can be additionally eliminated from the Dry EBM.

3 Results

The climate response to a radiative forcing in the Moist EBM and GCM organize into three groupings (Figure 1a,b). Climate change with a simple ice-albedo feedback, either with or without seasons, exhibits the greatest polar amplification. The addition of ice thermodynamics with seasons reduces warming at all latitudes and reduces polar amplification, particularly in the EBM. When ice thermodynamics without seasons is included, on the other hand, the response is identical (GCM) and nearly identical (EBM) to the climate response with a simple ice-albedo feedback (not shown), and in what follows we limit the thermodynamic-ice simulations to the seasonal case only. The amount of polar amplification for these icy regimes is comparable between the EBM and GCM, with a polar amplification factor of 3-4.

Climate change in the absence of ice, either with or without seasons, is characterized by less polar amplification than in the presence of ice feedbacks (orange lines in Fig. 1a,b). The result that polar amplification is merely reduced rather than eliminated is consistent with prior studies with moist EBMs (Roe et al., 2015; Merlis & Henry, 2018; Armour et al., 2019). However, that reduction is substantially less in the GCM, which overall exhibits less range in climate responses. Because the change in net solar radiation is zero in the ice-free EBM and GCM, the different responses must ultimately derive from differences in the model representations of atmospheric energy transport (i.e., diffusive in the EBM versus macroturbulent in the GCM) or the presence of a lapse rate feedback in the GCM. Notably, the inclusion of seasons in these idealized simulations has no effect on the magnitude and structure of annual-mean warming.

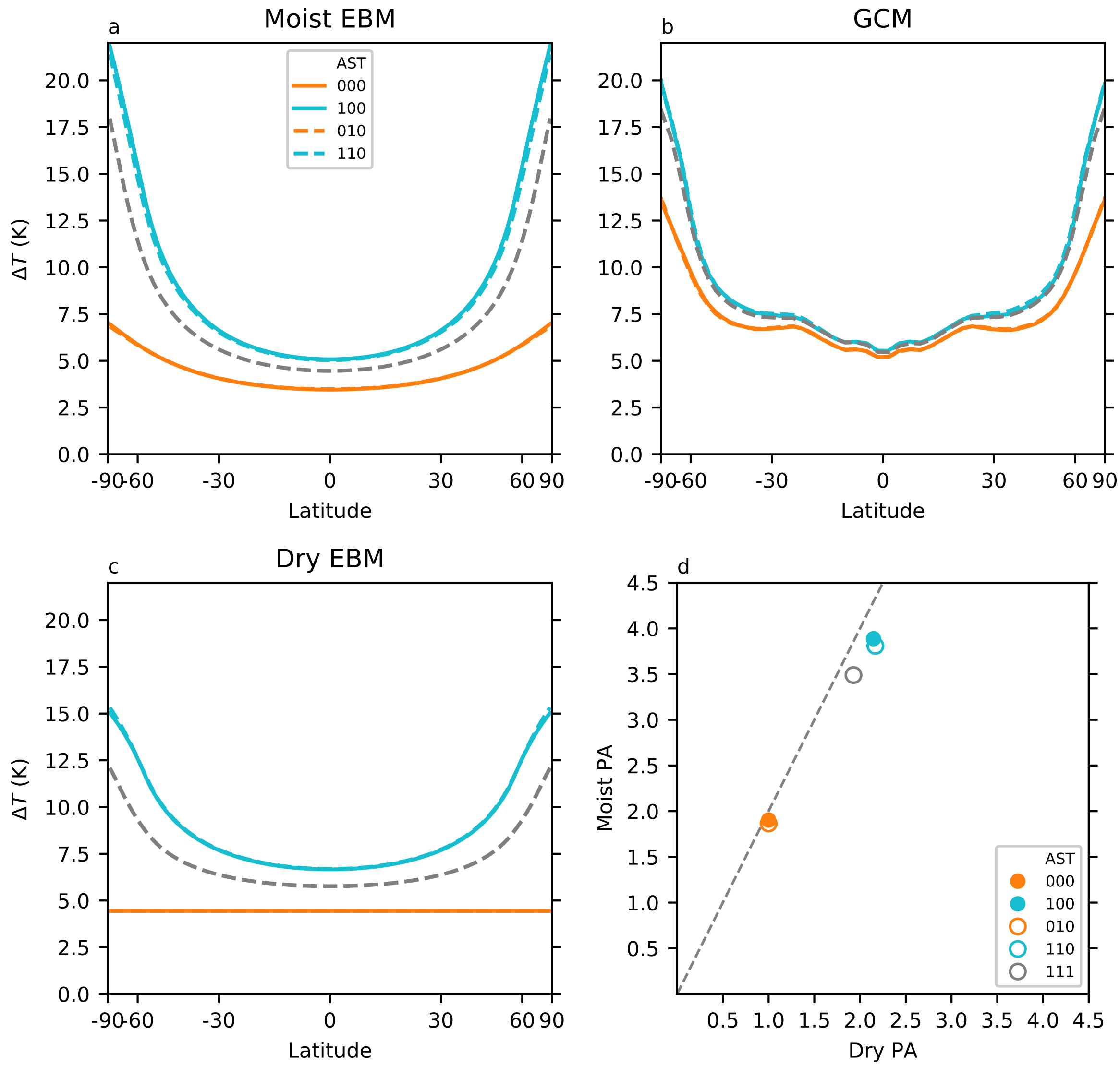

Figure 1. Polar amplification in the Moist EBM, GCM, and Dry EBM. (a) Annual-mean temperature response to an 8 W m^{-2} radiative forcing in the Moist EBM. (b) Annual-mean zonal-mean surface air temperature response to a 50% increase in longwave optical thickness in the GCM. (c) Annual-mean temperature response to an 8 W m^{-2} radiative forcing in the Dry EBM. (d) Polar amplification in the Moist EBM compared to the Dry EBM, where the polar amplification factor (PA) is calculated as the ratio of polar (65-90N) to tropical (0-6N) warming. The grey dashed reference line has a slope of 2. Simulation codes in the legend indicate whether ice albedo (A), seasonal cycle of insolation (S), or ice thermodynamics (T) are active: 000 (ice free), 010 (ice free with seasons), 100 (simple ice-albedo feedback), 110 (simple ice-albedo feedback with seasons), 111 (ice thermodynamics with seasons).

To understand why polar amplification is reduced in the Moist EBM with ice thermodynamics, we compare the seasonal cycle of temperature change across the sub-hierarchy of icy simulations (Fig. 2, top). The reduced amplification is clearly revealed to be a summer phenomenon (Fig. 2b,c). Examination of the climatological position of the ice line shows that thermodynamic ice has greater seasonal variability: the seasonal sea-ice maximum extends to the same latitude as for a simple ice-albedo feedback, however, the seasonal sea-ice minimum exhibits climatologically less ice. Hence, when subjected to a radiative forcing, there is less ice retreat, a smaller increase in net solar radiation (Fig. 3a), and less polar warming in the warm season. In contrast, during the cold season, polar amplification is enhanced by thermodynamic-ice processes. This disparate response is due not to a greater increase in net solar radiation (they are the same; Fig. 3a), nor to a weaker decrease in polar MSE flux convergence (Fig. 3c). Rather, the presence of ice thermodynamics results in a much colder base climate state (Fig. 3e), necessitating a larger temperature change when that ice melts. When the ice loss is prescribed as a forcing (Fig. 2d), the resulting melting explains essentially all of the summer polar warming and is approximately 4 K less than the total response to a radiative forcing (cf. Fig. 2c).

These two characteristics of thermodynamic ice—small ice extent during the warm season and thick, cold ice during the cold season—are both a consequence of the nonlinear growth rate of ice (4). Thin ice grows *and* melts faster than thick ice. However, the melt case is limited because once T_0 warms to the melting point, $T = T_m$. Freezing ice has no such temperature constraint. Hence, the effect of ice thermodynamics is to permit large seasonal excursions in ice extent characterized by summer temperatures near the melting point, by thin warm-season ice, and by thick cold-season ice with surface temperatures substantially below the freezing point. As noted by Eisenman and Wettlaufer (2009), the nonlinearity also allows stable seasonally ice-free climate states. Indeed, in simulations with more modest climate changes where ice persists in the cold season (not shown), the same mechanism determining the seasonal cycle of temperature change applies because the difference between the surface air and freezing temperature decreases with the ice thickness (4). The small-forcing warming pattern is thus also characterized by minimal summer warming and, when cold-season ice thins and partially retreats, enhanced warming.

The seasonal cycle of polar amplification is expressed differently with a simple ice-albedo feedback. Polar warming reaches its maximum in the warm season and its minimum in the cold season (Fig. 2b). A warm-season polar warming maximum can be explained by substantial ice retreat and, as a consequence, a large increase in net solar radiation (Fig. 3a). Additionally, the increase in absorbed solar radiation goes directly to raising temperatures rather than to melting ice. However, in neglecting the thermodynamic-ice processes described above, the seasonality of warming becomes inconsistent with comprehensive simulations and observations of polar warming. Hence, caution should be exercised when applying the moist, seasonal EBM with a simple ice-albedo feedback beyond the annual-mean climate response.

The seasonal cycle of temperature change in the GCM sub-hierarchy (Fig. 2, bottom) is broadly consistent with the Moist EBM. For a simple ice-albedo feedback, the seasonal cycle of ice extent is muted (Fig. 2f), and extensive ice retreat occurs in all seasons. Polar warming is greatest in the warm season, attendant with a relatively large increase in TOA net SW radiation (Fig. 3b) that is less than the EBM change in net solar radiation due to a smaller contrast in coalbedo of ocean and ice. Including thermodynamic-ice processes makes conditions less favorable for the maintenance of warm-season ice in the mean state. Hence, the increase in TOA net SW radiation (Fig. 3b) and polar warming (Fig. 2g) are relatively weak in the warm season, and it is the loss of thick cold-season ice (Fig. 3f) that produces substantial polar warming. In contrast to the Moist EBM, the summer polar warming in the GCM is not as strongly reduced by the presence of

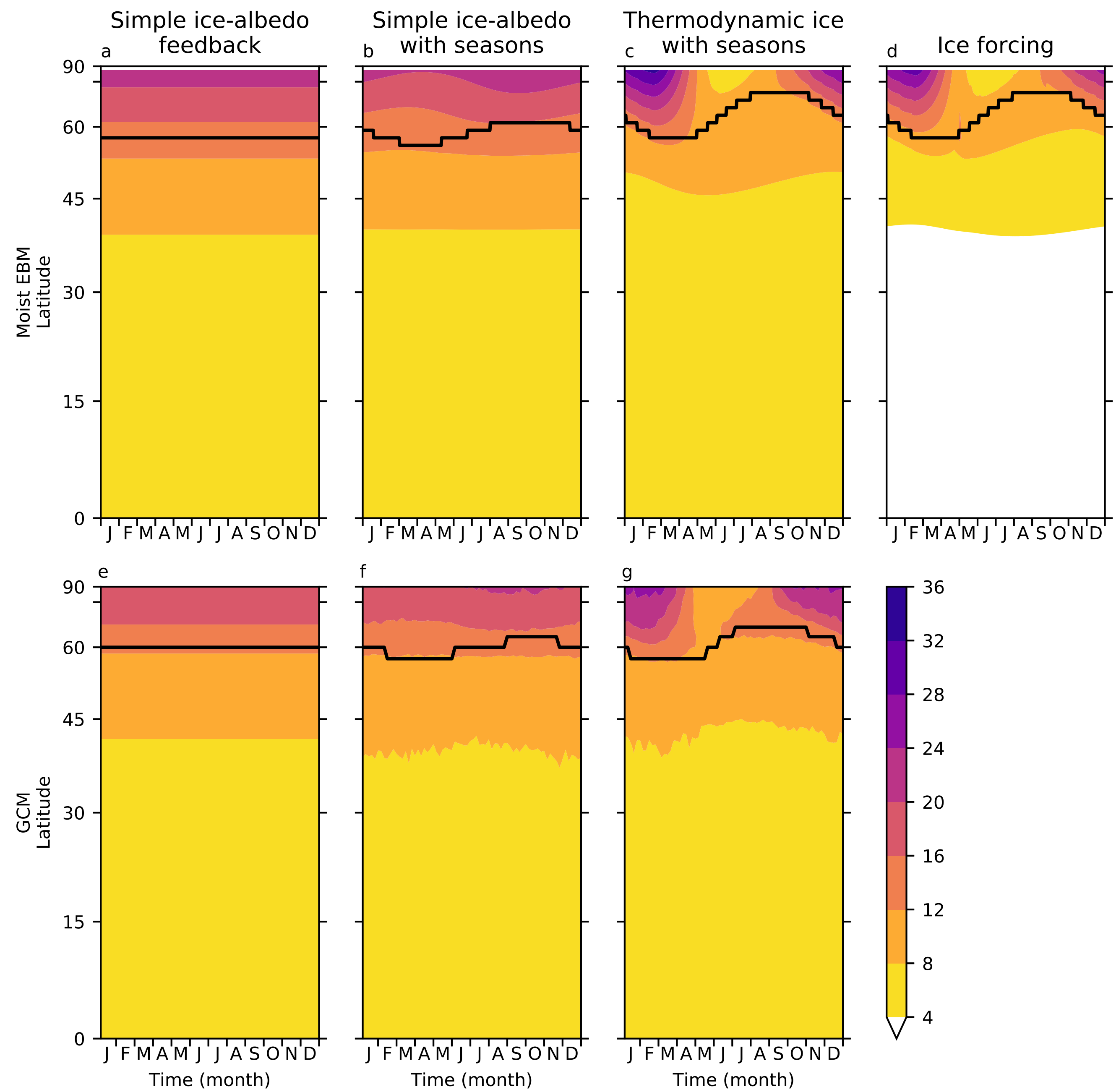

Figure 2. Seasonal cycle of temperature change in the Moist EBM and GCM in the presence of (a,e) a simple ice-albedo feedback (annual-mean insolation), (b,f) a simple ice-albedo feedback, and (c,g) ice thermodynamics. The black contour is the position of the climatological ice line (0% sea-ice concentration contour). As in Fig. 1, the GCM's surface air temperature is shown. (d) Seasonal cycle of temperature change for prescribed ice loss and constant radiative forcing ($\mathcal{F} = 8$ W m^{-2}). The temperature response to ice forcing is calculated as the difference between a Moist EBM simulation with freely evolving thermodynamic ice and a simulation with ice locked to its mean-state location and thickness.

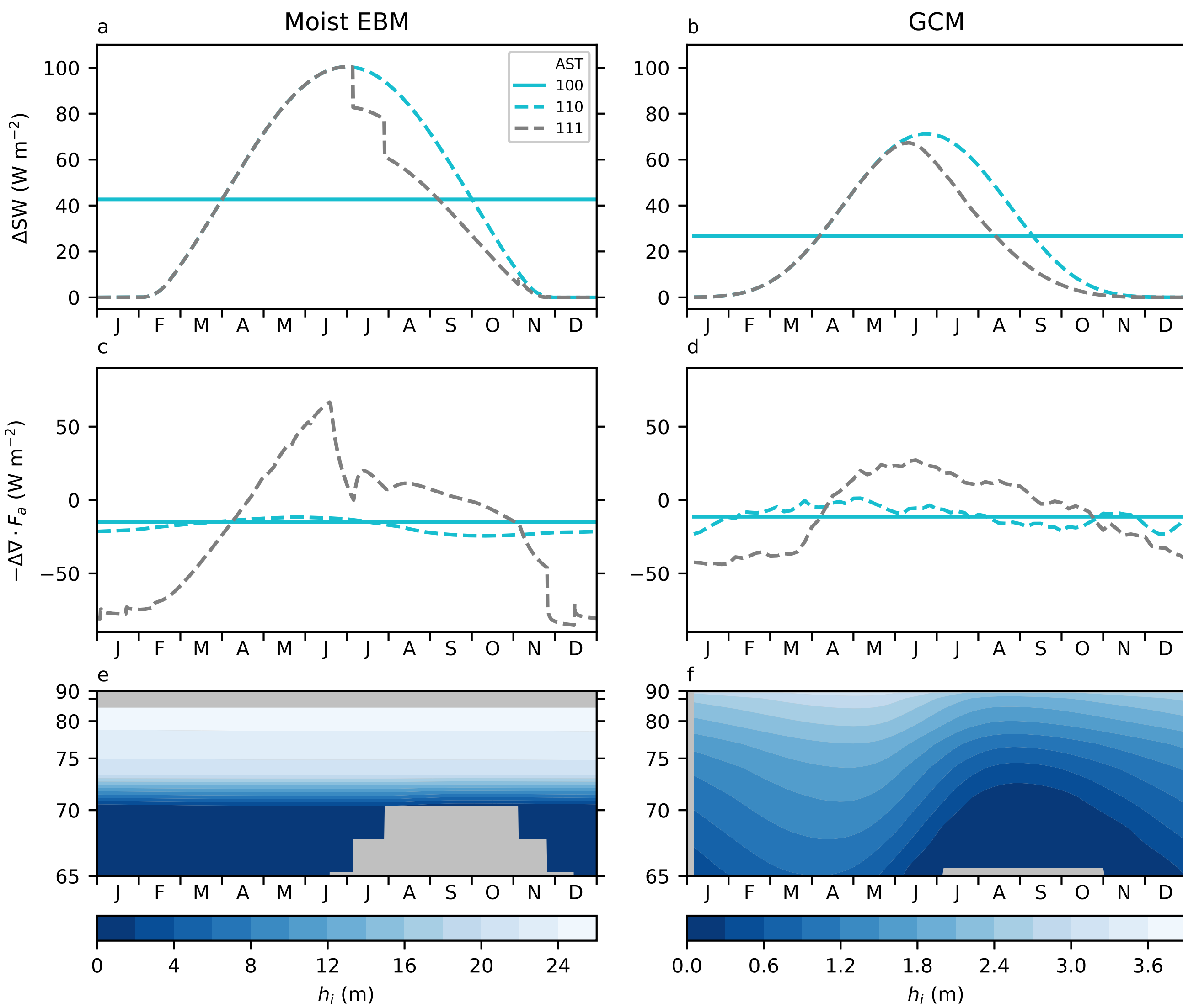

Figure 3. Change in polar energy flux diagnostics and climatological ice thickness for the Moist EBM and GCM. (a,b) Change in TOA net shortwave radiation (65-90N) in the presence of a simple ice-albedo feedback (100; annual-mean insolation), a simple ice-albedo feedback (110), and ice thermodynamics (111). (c,d) Change in convergence of MSE flux (65-90N) for the same simulations as in (a,b), with a one-month running mean applied to the GCM polar-average change in MSE flux convergence. (e,f) Ice thickness in simulations with ice thermodynamics.

ice thermodynamics, and, accordingly, the annual-mean temperature changes are less sensitive to different representations of ice processes (Fig. 1). Additionally, summertime exhibits a substantial increase in convergence of MSE flux into polar regions that is essentially absent for a simple ice-albedo feedback (Fig. 3d). The seasonal transition from anomalous convergence to anomalous divergence is consistent with the much greater weakening of MSE gradients under strong cold-season polar amplification.

We disable latent heat transport to elucidate the extent to which moist atmospheric processes and sea-ice processes interact to determine annual-mean polar amplification. In the Dry EBM, polar amplification is reduced across the hierarchy (Fig. 1c). The poles systematically warm less, and the tropics warm more. The previously identified groupings remain: climate change with a simple ice-albedo feedback exhibits greatest polar amplification, climate change with ice thermodynamics exhibits moderate polar amplification, and climate change in the absence of ice produces no polar amplification. As before, the presence of seasons has no effect on the magnitude and structure of warming. Notably, polar amplification in the Dry EBM is approximately half that of the Moist EBM. If the ice-albedo feedback and latent heat transport were perfectly additive in their contributions to polar amplification, then we would expect each to produce, for instance, a doubling and their combined contribution to produce a quadrupling; in other words, we would expect the amplification factors in Figure 1c to fall along the 2:1 line. Starting from the ice-free Dry EBM (PA = 1), adding latent heat transport has a slightly smaller influence (PA = 1.90) than adding a simple ice-albedo feedback (PA = 2.15), and their combined influence (PA = 3.89) is slightly less than their sum for the Moist EBM without seasons. A linear least-squares regression yields a slope of 1.7 across the range of representations of ice processes (not shown).

4 Conclusions

In this study, we have exploited a gap in climate model simulations to elucidate the role of, and interactions between, ice processes, the seasonal cycle, and moist processes in determining the polar-amplified pattern of warming. Further, we systematically compare the representation of the atmospheric flow: an idealized global circulation model resolves the atmospheric macroturbulence, while a diffusive energy balance model represents the net effect of this large-scale turbulence as a down-gradient, diffusive process. These simulations reveal that the inclusion of an ice-albedo feedback via a simple temperature-dependent surface albedo promotes polar amplification in the annual mean, as expected, however, the seasonal cycle of the temperature response exhibits a warm-season maximum that is inconsistent with comprehensive climate model projections. Adding complexity to the sea-ice processes in the form of a vertical heat flux upward through the ice modestly offsets the annual-mean polar-amplified warming and profoundly affects the seasonal cycle of polar-amplified warming. In these thermodynamic-ice simulations, enhanced winter warming occurs in both the EBM and GCM, a finding previously identified by Held (1982).

The seasonal cycle of insolation has essentially no effect on annual-mean polar amplification (in contrast to comprehensive models that include cloud radiative feedbacks, e.g., Kim et al., 2018) and little effect on the seasonality of polar-amplified warming—until sea-ice thermodynamic processes are included. Here, the seasonal polar warming arises as a consequence of the climatological ice state, which is characterized by large seasonal excursions in ice extent. Thin ice thins seasonally in summer while constrained to the melting point, and thin ice thickens in winter, promoting very cold surface temperatures (Eisenman & Wettlaufer, 2009). Hence, under radiatively forced warming, the melting of thick ice produces a much larger temperature response than the melting of thin ice. The seasonality of polar-amplified warming may equivalently be understood in terms of the different heat capacities of ice and water: ice loss enhances the sensitivity of wintertime temperature by eliminating the temperature difference between atmosphere and ocean, i.e., by increasing the effective surface heat capacity. Hence the climate transition from thick ice to water, as illustrated in the EBM, is characterized by more energy that goes into melting summertime ice than raising temperatures, large wintertime heat capacity changes, and large seasonal variations in the temperature response. The smaller seasonal warming variability in the GCM is consistent with a transition from relatively thin ice to water, though we note that differences in radiative forcing may also contribute.

The role of moist energy transport is critical in giving rise to polar-amplified warming in the absence of ice feedbacks, consistent with prior studies (Roe et al., 2015; Merlis & Henry, 2018; Armour et al., 2019). Furthermore, the Moist EBM simulations have a factor of 1.7 greater polar amplification across the range of representations of ice processes relative to corresponding Dry EBM simulations. This is suggestive of a superposition: in isolation, ice processes amplify polar warming; in isolation, moist processes amplify polar warming; together, ice and moist processes lead to amplified polar warming that is comparable to the sum of the individual roles. Additionally, while the representation of atmospheric flow quantitatively influences the annual-mean polar amplification, qualitative sensitivities to different ice representations are similar in the EBM and GCM. Notably, in these simulations moist transport can directly influence polar warming, however, it cannot influence warming via the water vapor feedback (e.g., Henry et al., 2021) or cloud feedbacks (Yoshimori et al., 2017; Graversen & Langen, 2019).

In conclusion, our systematic investigations in two idealized models provide evidence that all three mechanisms, ice processes, moist processes, and the seasonal cycle of insolation, are crucial for capturing the annual-mean and, importantly, seasonal pattern of polar-amplified warming. While the seasonal insolation cycle has no effect on the annual-mean polar amplification with a simple ice-albedo feedback, neglecting it results in a lack of fidelity of the seasonal cycle of warming with respect to projections from comprehensive models. Furthermore, the seasonal solar forcing is fundamental in setting the climatolgoical thermodynamic ice state that preconditions the ice-albedo feedback under more realistic ice representations. That feedback is weaker than that of a simple ice-albedo feedback and would contribute less to polar warming using popular TOA diagnostic frameworks (e.g., Pithan & Mauritsen, 2014). However, the weak surface albedo feedback conceals large seasonal changes in temperature, which would tend to promote, given stable stratification of the lower troposphere, a positive wintertime lapse rate feedback (e.g., Feldl et al., 2020). Those temperature changes also fundamentally drive the seasonal changes in polar energy flux convergence and reflect the seasonal changes in surface heat storage. The importance of such processes in interactively determining the feedback justifies our approach of using a climatological energy balance model. While questions remain regarding cloud interactions, our findings of comparable and nearly additive contributions of the ice-albedo feedback and moist transport provide a basis for refined assessment of attributions of Arctic amplification.

Acknowledgments

We are grateful to Till Wagner, Ian Eisenman, and Xiyue (Sally) Zhang for providing EBM and GCM codes that enabled this research. Support was provided by National Science Foundation award AGS-1753034 (NF) and a Compute Canada/Canada Foundation for Innovation computing allocation and a Canada Research Chair (TMM). Datasets for this research are available at http://doi.org/10.5281/zenodo.4738006.

References

Alexeev, V. A., Langen, P. L., & Bates, J. R. (2005). Polar amplification of surface warming on an aquaplanet in "ghost forcing" experiments without sea ice feedbacks. *Climate Dynamics*, *24*, 655–666. doi: 10.1007/s00382-005-0018-3

Armour, K. C., Siler, N., Donohoe, A., & Roe, G. H. (2019). Meridional atmospheric heat transport constrained by energetics and mediated by large-scale diffusion. *Journal of Climate*, *32*(12), 3655–3680. doi: 10.1175/JCLI-D-18-0563.1

Bitz, C. M., & Roe, G. H. (2004). A mechanism for the high rate of sea ice thinning in the Arctic Ocean. *Journal of Climate*, *17*(18), 3623–3632. doi: 10.1175/1520-0442(2004)017⟨3623:AMFTHR⟩2.0.CO;2

Boeke, R. C., & Taylor, P. C. (2018). Seasonal energy exchange in sea ice retreat regions contributes to differences in projected Arctic warming. *Nature Communications*, *9*. doi: 10.1038/s41467-018-07061-9

Bonan, D. B., Armour, K. C., Roe, G. H., Siler, N., & Feldl, N. (2018). Sources of uncertainty in the meridional pattern of climate change. *Geophysical Research Letters*, *45*, 9131–9140. doi: 10.1029/2018GL079429

Budyko, M. I. (1969). The effect of solar radiation variations on the climate of the Earth. *Tellus*, *21*, 611–619. doi: 10.3402/tellusa.v21i5.10109

Dai, A., Luo, D., Song, M., & Liu, J. (2019). Arctic amplification is caused by sea-ice loss under increasing CO2. *Nature Communications*, *10*, 121. doi: 10.1038/s41467-018-07954-9

Eisenman, I., & Wettlaufer, J. S. (2009). Nonlinear threshold behavior during the loss of Arctic sea ice. *Proceedings of the National Academy of Sciences of the United States of America*, *106*(1), 28–32. doi: 10.1073/pnas.0806887106

Feldl, N., Bordoni, S., & Merlis, T. M. (2017). Coupled high-latitude climate feedbacks and their impact on atmospheric heat transport. *Journal of Climate*, *30*(1), 189–201. doi: 10.1175/JCLI-D-16-0324.1

Feldl, N., Po-Chedley, S., Singh, H. K., Hay, S., & Kushner, P. J. (2020). Sea ice and atmospheric circulation shape the high-latitude lapse rate feedback. *npj Climate and Atmospheric Science*, *3*. doi: 10.1038/s41612-020-00146-7

Flannery, B. P. (1984). Energy balance models incorporating transport of thermal and latent energy. *Journal of the Atmospheric Sciences*, *41*(3), 414–421. doi: 10.1175/1520-0469(1984)041⟨0414:EBMITO⟩2.0.CO;2

Frierson, D. M. W., Held, I. M., & Zurita-Gotor, P. (2006). A gray-radiation aquaplanet moist GCM. Part I: Static stability and eddy scale. *Journal of the Atmospheric Sciences*, *63*(10), 2548–2566. doi: 10.1175/JAS3753.1

Frierson, D. M. W., Held, I. M., & Zurita-Gotor, P. (2007). A gray-radiation aquaplanet moist GCM. Part II: Energy transports in altered climates. *Journal of the Atmospheric Sciences*, *64*(5), 1680–1693. doi: 10.1175/JAS3913.1

Graversen, R. G., & Langen, P. L. (2019). On the role of the atmospheric energy transport in 2CO2-induced polar amplification in CESM1. *Journal of Climate*, *32*(13), 3941–3956. doi: 10.1175/JCLI-D-18-0546.1

Held, I. M. (1982). Climate models and the astronomical theory of the ice ages. *Icarus*, *50*(2-3), 449–461. doi: 10.1016/0019-1035(82)90135-X

Henry, M., Merlis, T. M., Lutsko, N. J., & Rose, B. E. (2021). Decomposing the Drivers of Polar Amplification with a Single Column Model. *Journal of Climate*, *34*(6), 2355–2365. doi: 10.1175/jcli-d-20-0178.1

Holland, M. M., & Bitz, C. M. (2003). Polar amplification of climate change in coupled models. *Climate Dynamics*, *21*, 221–232. doi: 10.1007/s00382-003-0332-6

Hwang, Y.-T., & Frierson, D. M. W. (2010). Increasing atmospheric poleward energy transport with global warming. *Geophysical Research Letters*, *37*(24). doi: 10.1029/2010GL045440

Hwang, Y.-T., Frierson, D. M. W., & Kay, J. E. (2011). Coupling between Arctic feedbacks and changes in poleward energy transport. *Geophysical Research Letters*, *38*(17). doi: 10.1029/2011GL048546

Kim, D., Kang, S. M., Shin, Y., & Feldl, N. (2018). Sensitivity of polar amplification to varying insolation conditions. *Journal of Climate*, *31*(12), 4933–4947. doi: 10.1175/JCLI-D-17-0627.1

Langen, P. L., Graversen, R. G., & Mauritsen, T. (2012). Separation of contributions from radiative feedbacks to polar amplification on an aquaplanet. *Journal of Climate*, *25*(8), 3010–3024. doi: 10.1175/JCLI-D-11-00246.1

Lutsko, N. J., Seeley, J. T., & Keith, D. W. (2020). Estimating impacts and trade-offs in solar geoengineering scenarios with a moist energy balance model. *Geophysical Research Letters*, *47*, e2020GL087290. doi: 10.1029/2020GL087290

Manabe, S., & Wetherald, R. T. (1975). The effects of doubling the CO2 concentration on the climate of a general circulation model. *Journal of the Atmospheric Sciences*, *32*(1), 3–15.

Merlis, T. M. (2014). Interacting components of the top-of-atmosphere energy balance affect changes in regional surface temperature. *Geophysical Research Letters*, *41*, 7291–7297. doi: 10.1002/2014GL061700

Merlis, T. M., & Henry, M. (2018). Simple estimates of polar amplification in moist diffusive energy balance models. *Journal of Climate*, *31*(15), 5811–5824. doi: 10.1175/JCLI-D-17-0578.1

North, G. R. (1975). Theory of energy-balance climate models. *Journal of the Atmospheric Sciences*, *32*(11), 2033–2043. doi: 10.1175/1520-0469(1975)032⟨2033:TOEBCM⟩2.0.CO;2

North, G. R., Cahalan, R. F., & Coakley, J. A. (1981). Energy balance climate models. *Reviews of Geophysics*, *19*(1), 91. doi: 10.1029/RG019i001p00091

O'Gorman, P. A., & Schneider, T. (2008). The hydrological cycle over a wide range of climates simulated with an idealized GCM. *Journal of Climate*, *21*(15), 3815–3832. doi: 10.1175/2007JCLI2065.1

Pithan, F., & Mauritsen, T. (2014). Arctic amplification dominated by temperature feedbacks in contemporary climate models. *Nature Geoscience*, *7*(3), 181–184. doi: 10.1038/ngeo2071

Roe, G. H., Feldl, N., Armour, K. C., Hwang, Y.-T., & Frierson, D. M. W. (2015). The remote impacts of climate feedbacks on regional climate predictability. *Nature Geoscience*, *8*(2), 135–139. doi: 10.1038/ngeo2346

Rose, B. E. J., Armour, K. C., Battisti, D. S., Feldl, N., & Koll, D. D. B. (2014). The dependence of transient climate sensitivity and radiative feedbacks on the spatial pattern of ocean heat uptake. *Geophysical Research Letters*, *41*. doi: 10.1002/2013GL058955

Russotto, R. D., & Biasutti, M. (2020). Polar amplification as an inherent response of a circulating atmosphere: Results from the TRACMIP aquaplanets. *Geophysical Research Letters*, *47*(6), e2019GL086771. doi: 10.1029/2019GL086771

Sellers, W. D. (1969). A global climatic model based on the energy balance of the Earth-atmosphere system. *Journal of Applied Meteorology*, *8*(3), 392–400. doi: 10.1175/1520-0450(1969)008⟨0392:agcmbo⟩2.0.co;2

Wagner, T. J. W., & Eisenman, I. (2015). How climate model complexity influences sea ice stability. *Journal of Climate*, *28*(10), 3998–4014. doi: 10.1175/jcli-d-14-00654.1

Winton, M. (2006). Amplified Arctic climate change: What does surface albedo feedback have to do with it? *Geophysical Research Letters*, *33*(3). doi: 10.1029/2005GL025244

Yoshimori, M., Abe-Ouchi, A., & Laîné, A. (2017). The role of atmospheric heat transport and regional feedbacks in the Arctic warming at equilibrium. *Climate Dynamics*, *49*(9-10), 3457–3472. doi: 10.1007/s00382-017-3523-2

Zhang, X., Schneider, T., Shen, Z., Pressel, K., & Eisenman, I. (submitted). Seasonal cycle of idealized polar clouds: Large eddy simulations driven by a GCM. *Journal of Advances in Modeling Earth Systems*.